

First measurement of massive virtual photon emission from N* baryon resonances

R. Abou Yassine^{6,14}, J. Adamczewski-Musch⁵, O. Arnold^{10,9}, E.T. Atomssa¹⁴, M. Becker¹¹, C. Behnke⁸, J.C. Berger-Chen^{10,9}, A. Blanco¹, C. Blume⁸, M. Böhmer¹⁰, L. Chlad^{15,c}, P. Chudoba¹⁵, I. Ciepal³, C. Deveaux¹¹, D. Dittert⁶, J. Dreyer⁷, E. Epple^{10,9}, L. Fabbietti^{10,9}, P. Fonte^{1,a}, C. Franco¹, J. Friese¹⁰, I. Fröhlich⁸, J. Förtsch¹⁸, T. Galatyuk^{6,5}, J. A. Garzón¹⁶, R. Gernhäuser¹⁰, R. Greifeuhagen^{7,b,*}, M. Grunwald¹⁷, M. Gumberidze⁵, S. Harabasz⁶, T. Heinz⁵, T. Hennino¹⁴, C. Höhne^{11,5}, F. Hojeij¹⁴, R. Holzmann⁵, M. Idzik², B. Kämpfer^{7,b}, K-H. Kampert¹⁸, B. Kardan⁸, V. Kedych⁶, I. Koenig⁵, W. Koenig⁵, M. Kohls⁸, B. W. Kolb⁵, G. Korcyl⁴, G. Kornakov¹⁷, F. Kornas^{6,5}, R. Kotte⁷, W. Krueger⁶, A. Kugler¹⁵, T. Kunz¹⁰, R. Lalik⁴, K. Lapidus^{10,9}, S. Linev⁵, L. Lopes¹, M. Lorenz⁸, T. Mahmoud¹¹, L. Maier¹⁰, A. Malige⁴, J. Markert⁵, S. Maurus¹⁰, V. Metag¹¹, J. Michel⁸, D.M. Mihaylov^{10,9}, V. Mikhaylov^{15,d}, A. Molenda², C. Müntz⁸, R. Münzer^{10,9}, L. Naumann⁷, K. Nowakowski⁴, J.-H. Otto¹¹, Y. Parpottas¹², M. Parschau⁸, C. Pauly¹⁸, V. Pechenov⁵, O. Pechenova⁵, J. Pietraszko⁵, T. Povar¹⁸, A. Prozorov^{15,c}, W. Przygoda⁴, K. Pysz³, B. Ramstein¹⁴, N. Rathod⁴, P. Rodriguez-Ramos^{15,d}, A. Rost^{6,5}, P. Salabura⁴, T. Scheib⁸, N. Schild⁶, K. Schmidt-Sommerfeld¹⁰, H. Schuldes⁸, E. Schwab⁵, F. Scozzi^{6,14}, F. Seck⁶, P. Sellheim⁸, J. Siebenson¹⁰, L. Silva¹, U. Singh⁴, J. Smyrski⁴, S. Spataro^e, S. Spies⁸, M.S. Stefaniak¹⁷, H. Ströbele⁸, J. Stroth^{8,5}, P. Strzempek⁴, C. Sturm⁵, K. Sumara⁴, O. Svoboda¹⁵, M. Szala⁸, P. Tlusty¹⁵, M. Traxler⁵, H. Tsertos¹³, O. Vazquez-Doce^{10,9}, V. Wagner¹⁵, A.A. Weber¹¹, C. Wendisch⁵, M.G. Wiebusch⁵, J. Wirth^{10,9}, H.P. Zbroszczyk¹⁷, E. Zherebtsova^{5,f}, P. Zumbach⁵

(HADES collaboration)

¹LIP-Laboratório de Instrumentação e Física Experimental de Partículas, 3004-516 Coimbra, Portugal

²AGH University of Science and Technology, Faculty of Physics and Applied Computer Science, 30-059 Kraków, Poland

³Institute of Nuclear Physics, Polish Academy of Sciences, 31342 Kraków, Poland

⁴Smoluchowski Institute of Physics, Jagiellonian University of Cracow, 30-059 Kraków, Poland

⁵GSI Helmholtzzentrum für Schwerionenforschung GmbH, 64291 Darmstadt, Germany

⁶Technische Universität Darmstadt, 64289 Darmstadt, Germany

⁷Institut für Strahlenphysik, Helmholtz-Zentrum Dresden-Rossendorf, 01314 Dresden, Germany

⁸Institut für Kernphysik, Goethe-Universität, 60438 Frankfurt, Germany

⁹Excellence Cluster 'Origin and Structure of the Universe', 85748 Garching, Germany

¹⁰Physik Department E62, Technische Universität München, 85748 Garching, Germany

¹¹II. Physikalisches Institut, Justus Liebig Universität Giessen, 35392 Giessen, Germany

¹²Frederick University, 1036 Nicosia, Cyprus

¹³Department of Physics, University of Cyprus, 1678 Nicosia, Cyprus

¹⁴Laboratoire de Physique des 2 infinis Irène Joliot-Curie, Université Paris-Saclay, CNRS-IN2P3, F-91405 Orsay, France

¹⁵Nuclear Physics Institute, The Czech Academy of Sciences, 25068 Rez, Czech Republic

¹⁶LabCAF. F. Física, Univ. de Santiago de Compostela, 15706 Santiago de Compostela, Spain

¹⁷Warsaw University of Technology, 00-662 Warsaw, Poland

¹⁸Bergische Universität Wuppertal, 42119 Wuppertal, Germany

and

M. Zetenyi¹⁹

¹⁹Wigner Research Centre for Physics, Budapest, Hungary

* Deceased

^aAlso at Coimbra Polytechnic - ISEC, Coimbra, Portugal

^bAlso at Technische Universität Dresden, 01062 Dresden, Germany

^cAlso at Charles University, Faculty of Mathematics and Physics, 12116 Prague, Czech Republic

^dAlso at Czech Technical University in Prague, 16000 Prague, Czech Republic

^eAlso at Dipartimento di Fisica and INFN, Università di Torino, 10125 Torino, Italy

^fAlso at University of Wrocław, 50-204 Wrocław, Poland

First information on the timelike electromagnetic structure of baryons in the second resonance region has been obtained from measurements of invariant mass and angular distributions in the quasi-free reaction $\pi^-p \rightarrow ne^+e^-$ at $\sqrt{s_{\pi^-p}} = 1.49$ GeV with the High Acceptance Di-Electron Spectrometer (HADES) detector at GSI using the pion beam impinging on a CH₂ target. We find a total cross section $\sigma(\pi^-p \rightarrow ne^+e^-) = 2.97 \pm 0.07^{data} \pm 0.21^{acc} \pm 0.31^{Z_{eff}} \mu\text{b}$. Combined with the Partial Wave Analysis of the concurrently measured two-pion channel, these data sets provide a crucial test of Vector Meson Dominance (VMD) inspired models. The commonly used "strict

VMD” approach strongly overestimates the e^+e^- yield. Instead, approaches based on a VMD amplitude vanishing at small e^+e^- invariant masses supplemented coherently by a direct photon amplitude provide a better agreement. A good description of the data is also obtained using a calculation of electromagnetic timelike baryon transition form factors in a covariant spectator-quark model, demonstrating the dominance of meson cloud effects. The angular distributions of e^+e^- pairs demonstrate the contributions of virtual photons with longitudinal polarization, in contrast to real photons. The virtual photon angular dependence supports the dominance of $J=3/2$, $I=1/2$ contributions observed in both the γ^*n and the $\pi\pi n$ channels.

Introduction. Hadrons are composite quantum objects, characterized by a number of parameters, such as mass, charge, spin or form factors, which derive from the strong-interaction. However, despite the impressive progress made by first-principle approaches, concerted actions of theory and experiment are still needed before they can be inferred directly from Quantum Chromodynamics (QCD). This motivates, in particular, the extensive studies of electromagnetic form factors for the transition between a nucleon (N) and baryon resonances (R) ($N\gamma^*\rightarrow R$) in the spacelike region, where the squared four-momentum q^2 of the virtual photon is negative, using meson electroproduction experiments [1–5]. However, a consistent understanding of baryon electromagnetic structure also requires experimental information in the timelike region $q^2 > 0$, which is very scarce [6–8]. The helicity amplitudes, or the closely related electromagnetic Transition Form Factors (eTFF), which encode the electromagnetic structure of involved baryons, are analytical functions of q^2 . Due to the crossing symmetry of the respective amplitudes the spacelike and timelike regions are connected by dispersion relations. The results obtained for various baryon transitions in the spacelike region reveal contributions from a quark core and a meson-cloud, being an important feature at small q^2 [9, 10]. The timelike kinematic domain can be addressed via the Dalitz decay of baryons ($R \rightarrow Ne^+e^-$), which probe electromagnetic transitions in the $q^2 = M_{e^+e^-}^2$ interval $[4m_e^2, (M_R - M_N)^2]$. Here $M_{e^+e^-}$ is the e^+e^- invariant mass and m_e , M_R and M_N are the electron, resonance and nucleon masses, respectively. Light vector mesons (VM= ρ and ω) should play a significant role, as suggested by the Vector Meson Dominance (VMD) models which assume that the photons couple to hadrons via a VM [11–13]. In contrast to neutral meson Dalitz decays [14–17], the applicability of VMD and its various extensions has not been explored so far for the description of timelike baryon transitions. Calculations of baryon eTFF based on the quark model apply VMD to describe the coupling of the photon to the constituent quark core and to the meson cloud. The results reveal the dominant role of the latter, with the ρ meson saturating the transition. eTFF of baryons are also studied by means of effective field, Dyson-Schwinger or lattice QCD approaches, which investigate the connection between VMD and the microscopic properties of QCD [18, 19].

Studies of photon-baryon couplings are also important

for the description of e^+e^- emission in elementary or heavy-ion collisions [20–23], where the dominance of ρ mesons (“strict VMD”) is commonly assumed. However, as pointed out in [24, 25], extended VMD versions, including either excited VM or a two-component photon coupling scheme (direct and via VM) seem to be more justified for the baryonic transitions. Furthermore, the experimentally established strong melting of the ρ meson in relativistic heavy-ion collisions [26–29] consistently confirms the predictions of hadronic models [30–34], which also strongly rely on the VMD applicability to photon-baryon couplings (for a recent review see [35]).

The aim of the present work is to scrutinise these various theoretical concepts. The recent HADES measurements of the $\pi^-p \rightarrow p\pi^-\pi^0$ and $\pi^-p \rightarrow n\pi^+\pi^-$ reactions analysed in the framework of the Bonn-Gachina Partial Wave Analysis (PWA) allowed to constrain the ρ production amplitudes [36], hence providing a reliable base to test VMD approaches on the corresponding e^+e^- spectrum.

In this letter, we present measurements of the quasi-free $\pi^-p \rightarrow ne^+e^-$ reaction at a center-of-mass energy $\sqrt{s_{\pi^-p}} = 1.49$ GeV/ c^2 using a CH₂ target, thus constituting the very first investigation of timelike electromagnetic structure of baryons in the second resonance region.

Experiment. A secondary pion beam with a central momentum of 0.685 GeV/ c was used. On average 10^5 pions/s with a momentum spread of $\pm 1.7\%$ were transported by the beam line [37] up to the target. Polyethylene (CH₂) cylinders and 7-fold segmented carbon (C) targets, with a diameter of 12 mm each and a similar extension of 4.6 cm, were used in separate runs. A diamond detector, with an active area of 14×14 mm, placed in front of the target, was used to trigger the data acquisition on incoming pions and to deliver a start signal for time-of-flight measurements. HADES [38] has excellent reconstruction capabilities for e^+e^- pairs. It consists of six identical sectors covering polar angles between 18° and 85° with respect to the beam axis. The momentum vectors of produced particles are reconstructed by means of four drift chambers (MDC), two in front of and two behind the magnetic field region provided by six coils of a super-conducting toroid. The time-of-flight (TOF) is measured by Resistive Plate Counters and scintillators covering polar angles smaller and larger than 45° , respectively.

Four-momentum vectors of the e^+ and e^- are recon-

structed by combining the information provided by the hadron blind RICH detector, the tracking and TOF systems [38, 39]. To reject correlated e^+e^- pairs from γ conversion and to reduce systematic errors related to efficiency corrections, pairs with opening angles smaller than 9° or single lepton momenta smaller than $100 \text{ MeV}/c$ are rejected. The combinatorial background (CB), originating from the conversion of photons from π^0 decays, is subtracted bin-by-bin as described in Sec. S1 of [40]. In total, 16340 signal e^+e^- pairs have been reconstructed.

Efficiency corrections are calculated as a function of momenta, polar and azimuthal angles, using single-lepton correction matrices deduced from full simulations of the HADES detection system, resulting in an average correction factor of about 2. The acceptance for e^+e^- pairs with $M_{e^+e^-} > M_{\pi^0}$ is of the order of 20 %. The normalisation of measurements with the C and CH₂ targets is determined with a precision of 4%, as described in [36] (see also Sec. S2 of [40]).

Simulations. In the energy range of our experiment, three main sources of e^+e^- pairs are expected to contribute and were accordingly implemented in simulations: (i) the π^0 Dalitz decay ($\pi^0 \rightarrow \gamma e^+e^-$), (ii) the η Dalitz decay ($\eta \rightarrow \gamma e^+e^-$) and (iii) the exclusive $\pi^-p \rightarrow ne^+e^-$ reaction. The π^0 and η Dalitz decays were simulated using production cross sections from former experiments [41]. To generate e^+e^- events of the $\pi^-p \rightarrow ne^+e^-$ reaction, calculations were performed for the D_{13} and S_{11} partial waves, which dominate both the $\pi^-p \rightarrow \gamma n$ [42] and $\pi^-p \rightarrow \rho n$ [36] reactions and yield the same dependence of differential cross sections as a function of $M_{e^+e^-}$ [24, 41, 43]. The normalisation of this calculation was given by the known cross section of $\pi^-p \leftrightarrow \gamma n$ [42]. This approach, corresponding to a calculation of Dalitz decays involving two point-like baryons will be referred to as "QED reference". The effect of the unknown eTFF, which are expected to modify the yield in the ρ mass region, is estimated with a data-driven VMD approach using the ρ contribution extracted in the PWA of the $\pi^-p \rightarrow n \pi^+\pi^-$ reaction measured in the same experiment [36]. To calculate the corresponding e^+e^- yields, we developed Monte-Carlo simulations for the ρ production in the π^-p reaction and the subsequent ρ decay in both e^+e^- and $\pi^+\pi^-$ channels. The normalisation of these simulations is given by the ρ production cross section of 1.35 mb [36] and a 10% d-wave contribution is added to the dominant s-wave, for an accurate description of the $\pi^+\pi^-$ spectrum.

The partial decay width of the ρ meson into an e^+e^- pair, $\Gamma_{e^+e^-}(M)$, is calculated using the VMD1 and VMD2 approaches, as defined in [13], which are based on two different Lagrangians for the $\gamma - \rho$ coupling. Using the definition of the self-energy $Im\Sigma_\rho = M\Gamma_{tot}(M)$, the corresponding partial decay widths reads

$$\text{VMD1} : \Gamma(M_{e^+e^-})_{\text{VMD1}} = \Gamma_0 M_{e^+e^-} / M_0, \quad (1)$$

$$\text{VMD2} : \Gamma(M_{e^+e^-})_{\text{VMD2}} = \Gamma_0 (M_0 / M_{e^+e^-})^3, \quad (2)$$

respectively, where Γ_0 is the partial decay width at the Breit-Wigner mass M_0 . In the case of VMD1 [25, 44], the $\rho \rightarrow e^+e^-$ amplitude vanishes for small $M_{e^+e^-}$ and a direct photon coupling contribution is added. As emphasized in [13], VMD1 therefore presents by construction the advantage of allowing for a non universality of VM and electromagnetic couplings to hadrons. This is particularly significant in the baryon sector and is manifested by the strong overestimate of the radiative decay widths [45] when using VMD2 ("strict VMD"), commonly used in transport calculations [20–23]. On the other hand, predictions of e^+e^- yields using VMD1 in the region below the VM poles are sensitive to the phase between the photon and VM coupling amplitudes [46], which is a free parameter in our calculation.

An alternative approach, the eTFF model, is implemented, based on the recently developed quark model for eTFF for the N-N(1520) [47] and N-N(1535) [48] transitions. In practice, the $M_{e^+e^-}$ dependent differential cross sections from the "QED reference" are weighted by an effective squared eTFF, which depends on the squared moduli of the magnetic, electric and Coulomb form factors [47] and has a very similar shape for N-N(1520) and N-N(1535) transitions.

Interactions with carbon nuclei were treated in a quasi-free approach, using the participant-spectator model, assuming a spectator ^{11}B nucleus on the mass shell and taking into account the nucleon momentum distribution in carbon [49]. Details about the simulation procedure can be found in Sec. S3 and Sec. S4 of [40].

Invariant masses. For $M_{e^+e^-}$ larger than the π^0 mass, a cut on the e^+e^- missing mass $M_{miss} = \sqrt{(P_{in} - P_{out})^2}$, where $P_{in} = p_\pi + p_p$ and $P_{out} = p_{e^+} + p_{e^-}$, can be used to select the exclusive $\pi^-p \rightarrow ne^+e^-$ process (Fig. 1). P_{in} is calculated for a fixed pion momentum of $0.685 \text{ GeV}/c$ incident on a free proton at rest. The normalized distributions measured for the CH₂ (Fig. 1a) and C (Fig. 1b) targets have been subtracted to determine the distribution for π^-p interactions (Fig. 1c). The three distributions show two similar structures, which are well reproduced by the simulations: a peak around the neutron mass, which can be attributed to the exclusive $\pi^-p \rightarrow ne^+e^-$ reaction, either on a free proton or a bound proton in the carbon nuclei and a broader structure, primarily due to the η Dalitz decay. The width of the neutron peak obtained for the free $\pi^-p \rightarrow ne^+e^-$ reaction is mainly due to the detector resolution, with only a minor impact of the pion beam momentum spread, while, for the carbon target, it mainly results from the nucleon momentum distributions. For the π^-p reaction, the simulated yields directly result from measured cross section inputs, while the good description of the peak around the neutron mass confirms the consistency of the treatment of the $\pi^-p \rightarrow ne^+e^-$ process in the simula-

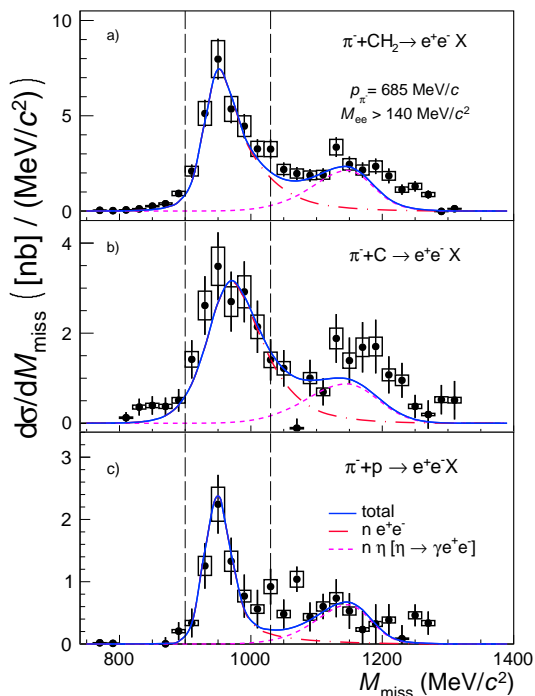


FIG. 1. Distribution of the missing mass M_{miss} calculated *w.r.t.* the π^-p system for a fixed pion beam momentum of 0.685 GeV/c for events with e^+e^- invariant mass larger than 140 MeV/c². Data (symbols with error bars) for $\pi^- + \text{CH}_2$ (a), $\pi^- + \text{C}$ (b) and $\pi^- + p$ (c) are displayed after efficiency corrections. Simulated distributions (histograms) after full reconstruction are shown for the $\pi^-p \rightarrow ne^+e^-$ channel using the eTFF model (dotted-dashed red), η Dalitz decay (dashed magenta) and the total (blue). The vertical dashed lines indicate the missing mass window used to select the $\pi^-p \rightarrow ne^+e^-$ reaction.

tion, where the effective eTFF model was used. The ratio of measured yields on CH₂ and carbon targets is used to extract a cross section ratio $\sigma_C/\sigma_p = 2.9 \pm 0.5$ (see Sec. S2 and Sec. S4 of [40] for details) which is applied in the simulation. In the quasi-free scenario, this ratio can be interpreted as the number of participant protons Z_{eff} in the carbon target and the result is in good agreement with the $A^{2/3}$ dependence observed in previous measurements of total reaction cross sections [50], considering e^+e^- production on the neutron as strongly suppressed at this energy. The second structure is well described by the simulation of the η Dalitz decay, although contributions from the Bremsstrahlung process, of the type $\pi^-N \rightarrow \pi N e^+e^-$, might be responsible for the missing yield above $M_{\text{miss}} = m_n + m_\pi$. Due to the low statistics recorded on the carbon target (Fig. 1b), the precision obtained separately for π^-p and $\pi^- + \text{C}$ interactions is limited and does not allow for a study of the corresponding distributions as a function of invariant mass or angles. Therefore, the focus of this analysis is on the polyethylene target measurements. The exclusive

quasi-free $\pi^-p \rightarrow ne^+e^-$ channel is selected by applying a missing mass selection ($900 < M_{\text{miss}} < 1030$ MeV/c²). As shown in Fig. 2a, the π^0 Dalitz decay is not fully suppressed by this missing mass cut. It is however well described by the simulation, which is therefore used to subtract its contribution. The further analysis is based on 1280 e^+e^- pairs with $M_{e^+e^-} > 100$ MeV/c², which remain after this subtraction. Acceptance correction factors were deduced in each 20 MeV/c² wide invariant mass bin, using the simulation with the eTFF model. The average correction amounts to 5.9 with a smooth invariant mass dependence. Due to the model dependence of this correction, the corrected yields are affected by a systematic error of 5%. According to the simulation, the yields are reduced by about 20%, due to the missing mass cut, which is not corrected for. To calculate cross sections for the quasi-free reaction $\pi^-p \rightarrow ne^+e^-$, the number of effective protons ($Z_{\text{eff}}+2$) contributing to the $\pi^- + \text{CH}_2$ reaction has been taken into account. The resulting invariant mass spectrum is compared to the result of our simulations in Fig. 2b. Below 200 MeV/c², the experimental cross section is in fair agreement with the QED reference. However, at larger invariant masses, an excess of up to a factor 5 is observed, pointing to a strong effect of the eTFF. To demonstrate this effect more directly, the ratios of data and simulations to the QED reference are displayed in Fig. 2c, which can be considered a measure of the effective eTFF in the $\pi^-p \rightarrow ne^+e^-$ reaction.

The various eTFF models presented above can then be confronted with these data. First, it is interesting to check the model based on the ρ contributions from the PWA analysis. The VMD2 version is found to give a reasonable description of yields measured for the highest invariant masses, but strongly overestimates the yields below 350 MeV/c², which clearly points to the limitation of the "strict VMD" model in the baryon sector. This important result shows the consequence of the "strict VMD" for the modeling of dilepton spectra and is related to the long standing problem of overestimating the radiative baryon decay widths. In the VMD1 approach, the ρ contribution, which is reduced by a factor $(M/M_\rho)^4$ *w.r.t.* VMD2, should be compared to the coherent sum of the ρ and γ contributions. As shown in Fig. 2b, the yields above 300 MeV/c² depend on the interference between the two amplitudes. An incoherent sum of the two contributions (thick cyan curve) significantly underestimates the data, but a better description of the e^+e^- invariant mass spectrum can be obtained using a maximum constructive interference (blue colored area). As shown by the hatched areas in Figs. 2b and c, the effect of the ρ -n d-wave contribution is mostly significant for the VMD2 model. To illustrate the effect of the Fermi motion in the carbon nucleus in the simulations, the yields calculated directly from the $\pi^-p \rightarrow \rho n$ PWA solution [36] are also shown as gray triangles up and blue triangles down for VMD2 and VMD1, respectively.

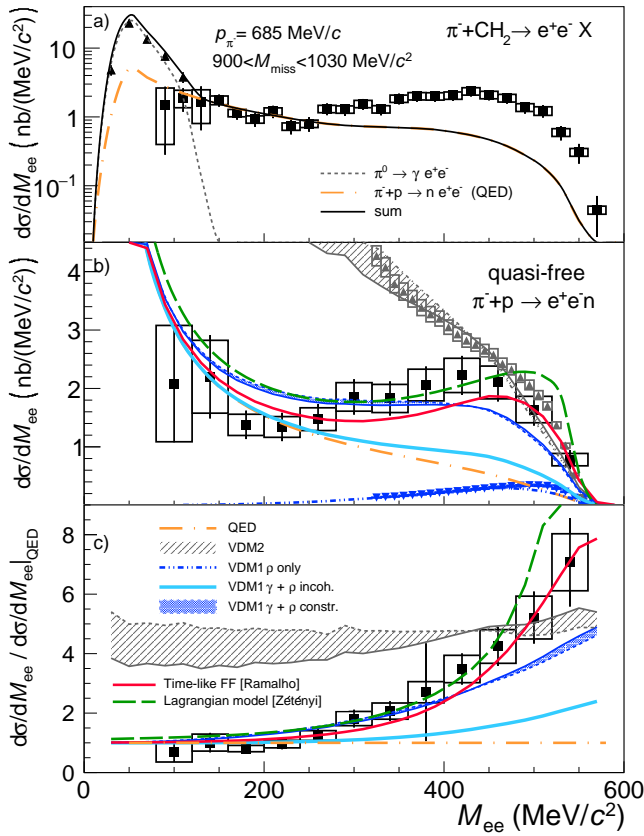


FIG. 2. (a) $d\sigma/dM_{e^+e^-}$ for the $\pi^- + \text{CH}_2$ reaction integrated in the HADES acceptance over the missing mass range [900-1030] MeV/c^2 . Full triangles: total yields, full squares: after subtraction of the π^0 Dalitz decay contribution ($\pi^0[\gamma e^+e^-]$). The curves display the simulations for point-like baryon Dalitz decay ("QED reference", orange dashed-dotted curve), π^0 Dalitz decay (black dotted curve) and the sum (black solid curve). (b) $d\sigma/dM_{e^+e^-}$ for the quasi-free $\pi^-p \rightarrow ne^+e^-n$ reaction integrated over the missing mass range [900-1030] MeV/c^2 after normalisation by the number of effective protons and acceptance corrections. Gray triangles up (blue triangles down): e^+e^- yields deduced from the $\pi^-p \rightarrow n\rho n$ PWA contribution [36] using VMD2 (VMD1). Orange dashed-dotted curve: QED reference ($(d\sigma/dM_{e^+e^-})_{\text{QED}}$), gray dashed area: VMD2 model with d-wave contribution varied from 0 (full curve) to 10% (dashed curve), blue colored area (cyan curve): same for VMD1 models with constructive (incoherent) sum of ρ and γ contributions, long dash-dot-dot-dashed blue curve: ρ contribution to the VMD1 model. Calculations using the timelike Form-Factor model (red solid curve) and the Lagrangian model (green long dashed curve) are also shown. (c) Ratios $(d\sigma/dM_{e^+e^-})/(d\sigma/dM_{e^+e^-})_{\text{QED}}$. The same marker and curve styles apply as in panel (b). Symbols with vertical and horizontal bars show the data with total and systematic point-to-point errors, respectively and curves display simulations with absolute normalisation in all panels.

Our results are also compared to the microscopic calculation of [46] based on an effective Lagrangian approach, taking into account various resonant and non-resonant amplitudes in a coherent way using the $N^*N\rho$ couplings

derived from the PWA [36]. A salient feature of this model is the application of the two-component VMD1 model to all baryon-photon couplings. Choosing a relative phase of 90° between the resonant γ and ρ amplitudes, a good description of the e^+e^- production is achieved, as shown by the green long dashed curve in Figs. 2b and c. The calculation was performed for the free $\pi^-p \rightarrow ne^+e^-$ reaction which might explain the peak-like structure at large invariant masses. One has however to consider that these calculations have not yet been confronted with the measured two-pion production. Moreover, this model accommodates a strong contribution of non-resonant Born terms in the dilepton production, in contrast to the PWA analysis of the $\pi^-p \rightarrow n\rho$ channel [36], where the main contributions are due to $N(1520)$ and (to a smaller extent) to $N(1535)$ excitation in the s-channel.

Simulations based on the eTFF model [47, 48] for these resonances also give a satisfactory description of the data, which demonstrates that the dominant meson cloud contribution is taken into account in a realistic way. As the evolution of the effective eTFF is mainly driven by the pion electromagnetic form factor, this calculation provides an independent VMD approach for the $\pi^-p \rightarrow ne^+e^-$ reaction.

The measured e^+e^- cross section for $M_{e^+e^-} \approx 500$ MeV/c^2 is more than two orders of magnitude larger than the calculations of [51], which were based on a very low off-shell ρ cross section and strong destructive interferences with off-shell ω production. The calculations of [52], which were performed for \sqrt{s} larger than 1.6 GeV, also predicted large negative interferences between ρ and ω , though with a larger ρ yield.

The "QED reference" model was used to extrapolate the experimental differential cross section at small invariant masses ($M_{e^+e^-} < 100$ MeV/c^2). In this way, a total cross section for the free $\pi^-p \rightarrow ne^+e^-$ reaction of $\sigma = (2.97 \pm 0.07^{\text{data}} \pm 0.21^{\text{acc}} \pm 0.31^{\text{Zeff}}) \mu\text{b}$ can be deduced, where the errors are due to uncertainties of the measurement, the acceptance correction and the effective number of protons, respectively. The ratio of the integrated experimental and "QED reference" cross sections, which can be attributed to an effective eTFF, amounts to 1.35 ± 0.03 (data) ± 0.02 (acceptance).

Angular distributions. Further information on the nature of the timelike electromagnetic transitions in the $\pi^-p \rightarrow ne^+e^-$ reaction can be obtained from the angular distributions. A convenient parameterization of the differential cross sections $d^4\sigma/d\Theta_{\gamma^*}dM_{e^+e^-}d\cos\Theta d\phi \propto |A|^2$ is provided by the density matrix formalism [46, 53, 54] with the relevant dependencies of the mod-squared amplitude at given value of $M_{e^+e^-}$ and polar angle (Θ_{γ^*}) of the virtual photon in the center-of-mass frame:

$$|A|^2 \propto 8k^2 [1 - \rho_{11} + (3\rho_{11} - 1) \cos^2 \Theta + \sqrt{2} \text{Re} \rho_{10} \sin 2\Theta \cos \phi + \text{Re} \rho_{1-1} \sin^2 \Theta \cos 2\phi]. \quad (3)$$

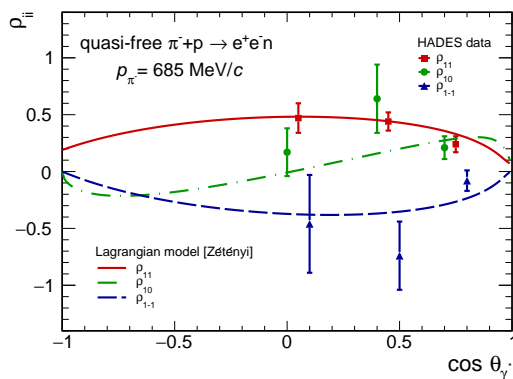


FIG. 3. Results of the analysis of the e^+ and e^- angular distributions in the quasi-free $\pi^-p \rightarrow ne^+e^-$ reaction at $\sqrt{s} = 1.49$ GeV. Spin density matrix elements ρ_{11} (red symbols), ρ_{10} (green symbols) and ρ_{1-1} (blue symbols) extracted for e^+e^- events with $M_{e^+e^-} > 300$ MeV/ c^2 , are compared to the predictions of the model [46] for ρ_{11} (full curve), ρ_{10} (dash-dotted curve) and ρ_{1-1} (dashed curve).

Here, k , Θ and ϕ denote the momentum, the polar and azimuthal angles of the electron in the virtual photon reference frame, respectively, and $\rho_{11,10,1-1}$ are the three independent density matrix coefficients. A method to extract these quantities from a fit to experimental data has been developed taking into account acceptance and detector inefficiency effects [41, 43, 54]. Although the statistics of the measurement is limited, the coefficients can be extracted as a function of the γ^* emission angle in the center-of-mass for $M_{e^+e^-} > 300$ MeV/ c^2 , as shown in Fig. 3. The significant deviations of ρ_{11} from 0.5 and ρ_{10} from 0 clearly demonstrate the contributions of virtual photons with longitudinal polarization, in contrast to real photons. The angular dependence of the coefficients indicate important contributions of spins larger than 1/2, in agreement with the dominance of the N(1520) resonance in the ρ production, which was found in the PWA of the two-pion production [36]. The results are also compared to the predictions of the Lagrangian model [46] for an invariant mass $M_{e^+e^-} = 400$ MeV/ c^2 and a phase $\phi = 90^\circ$ between the photon and ρ contribution, to be consistent with the comparison of invariant mass distributions (Fig. 2). The main trend of the data is accounted for, which indicates a realistic description of the virtual photon polarization and a dominant J=3/2 contribution in the model.

Summary. In summary, e^+e^- production has been measured for the first time in pion induced reactions at a momentum of 0.685 GeV/ c , opening a window on the timelike electromagnetic structure of baryon transitions in the second resonance region. The data for the quasi-free $\pi^-p \rightarrow ne^+e^-$ reaction are consistent with the $\pi^-p \rightarrow \gamma n$ results for invariant masses below 250 MeV/ c^2 , while an excess by up to a factor 5 is observed

for larger invariant masses, demonstrating the strong effect of eTFF. Taking advantage of the existing PWA solution for the two-pion production in the same experiment [36], a quantitative verification of models based on VMD could be achieved. In particular, a "strict VMD" approach, based on the VMD2 Lagrangian with mass independent $\gamma - \rho$ coupling constant [11], strongly overestimates the e^+e^- yield below 300 MeV/ c^2 . As VMD2 is widely used in several transport models, this result might have an important impact on predictions of e^+e^- yields in exclusive hadronic reactions or on calculations of the in-medium emission of e^+e^- pairs in heavy-ion reactions. The two-component approach, based on the coherent sum of a direct photon and a ρ amplitude derived from the VMD1 Lagrangian [13], allows for a better description of our data over the full e^+e^- invariant mass range. The nature of the transition, with a dominant contribution from N-N(1520) is corroborated by the extraction of the spin density matrix elements. A Lagrangian model based on the two-component approach for each resonant and non-resonant contribution, albeit with an apparently different interference scheme between the γ and ρ amplitudes than in our model provides a fair description of the invariant mass distribution and the spin density matrix elements. The strength of the Born term should however be confronted by the PWA results on two pion production. The effective eTFF which can be derived from our data is found to be in good agreement with the predictions of meson cloud effects in a covariant eTFF model [48, 55]. While these pioneering results call for systematic studies of baryon transitions with higher statistics using pion-induced e^+e^- production, the present data base can be already used as a crucial benchmark for the models of e^+e^- production and in-medium ρ meson spectral function.

We appreciated the theoretical tools provided by A. Sarantsev, G. Ramalho and T. Peña. We are also grateful for the interesting discussions on theoretical aspects with Kai Gallmeister and Ulrich Mosel. We acknowledge support from SIP JUC Cracow, Cracow (Poland), National Science Center, 2016/23/P/ST2/040 POLONEZ, 2017/25/N/ST2/00580, 2017/26/M/ST2/00600; TU Darmstadt, Darmstadt (Germany), DFG GRK 2128, DFG CRC-TR 211, BMBF:05P18RDFC1, HFHF, ELEMENTS:500/10.006, VH-NG-823, GSI F&E, ExtreMe Matter Institute EMMI at GSI Darmstadt; Goethe-University, Frankfurt (Germany), BMBF:05P12RFGHJ, GSIF&E, HIC for FAIR (LOEWE), ExtreMe Matter Institute EMMI at GSI Darmstadt; TU München, Garching (Germany), MLL München, DFG EClust 153, GSI TMLRG1316F, BmBF 05P15WOFCA, SFB 1258, DFG FAB898/2-2; JLU Giessen, Giessen (Germany), BMBF:05P12RGGHM; IJCLab Orsay, Orsay (France), CNRS/IN2P3, P2IO Labex, France; NPI CAS, Rez, Rez (Czech Republic), MSMT LM2018112, LTT17003, MSMT OP VVV CZ.02.1.01/0.0/0.0/18 046/0016066.

The following colleagues from Russian institutes did contribute to the results presented here but are not explicitly listed as authors following the decision of the HADES Collaboration Board on March 23, 2022: A. Belyaev, O. Fateev, M. Golubeva, F. Guber, A. Ierusalimov, A. Ivashkin, A. Kurepin, A. Kurilkin, P. Kurilkin, V. Ladygin, A. Lebedev, M. Mamaev, S. Morozov, O. Petukhov, A. Reshetin, A. Sadovsky, A. Shabanov, and A. Taranenkov.

-
- [1] I. G. Aznauryan *et al.*, Phys. Rev. **C80**, 055203 (2009), *Electroexcitation of nucleon resonances from CLAS data on single pion electroproduction.*
- [2] R. Thompson *et al.*, Phys. Rev. Lett. **86**, 1702 (2001), *The $ep \rightarrow e'p\eta$ reaction at and above the $S(11)(1535)$ baryon resonance.*
- [3] I. Aznauryan *et al.*, Int. J. Mod. Phys. **E22**, 1330015 (2013), *Studies of Nucleon Resonance Structure in Exclusive Meson Electroproduction.*
- [4] V. I. Mokeev *et al.*, Phys. Rev. **C93**, 025206 (2016), *New Results from the Studies of the $N(1440)1/2^+$, $N(1520)3/2^-$, and $\Delta(1620)1/2^-$ Resonances in Exclusive $ep \rightarrow e'p'\pi^+\pi^-$ Electroproduction with the CLAS Detector.*
- [5] E. L. Isupov *et al.*, Phys. Rev. **C96**, 025209 (2017), *Measurements of $ep \rightarrow e'\pi^+\pi^-p'$ Cross Sections with CLAS at $1.40 \text{ GeV} < W < 2.0 \text{ GeV}$ and $2.0 \text{ GeV}^2 < Q^2 < 5.0 \text{ GeV}^2$.*
- [6] S. Berezhnev, T. Blokhintseva, A. Demyanov, A. Kuptsov, V. Kurochkin, L. Nemenov, G. Smirnov, and D. Khazins, Sov. J. Nucl. Phys. **24**, 591 (1976), *The Measurement of the Pion and Nucleon Form-Factors in the Region of the Timelike 4-Momentum Transfers from 1.5 to 3.0 fm^{-2} .*
- [7] C. M. Hoffman, J. S. Frank, R. E. Mischke, D. C. Moir, J. S. Sarracino, P. A. Thompson, and M. A. Schardt, Phys. Rev. D **28**, 660 (1983), *A measurement of $\pi^-p \rightarrow ne^+e^-$ at 300 MeV/c and a search for scalar and vector bosons heavier than the π^0 .*
- [8] A. P. Ierusalimov and G. I. Lykasov, Phys. Part. Nucl. Lett. **15**, 457 (2018), *Dielectron Production in Pion-Nucleon Reactions at Intermediate Energies.*
- [9] B. Julia-Diaz, T. S. H. Lee, A. Matsuyama, T. Sato, and L. C. Smith, Phys. Rev. **C77**, 045205 (2008), *Dynamical coupled-channels effects on pion photoproduction.*
- [10] I. G. Aznauryan and V. Burkert, Phys. Rev. **C95**, 065207 (2017), *Electroexcitation of nucleon resonances of the $[70, 1^-]$ multiplet in a light-front relativistic quark model.*
- [11] J. J. Sakurai, Phys. Rev. Lett. **22**, 981 (1969), *Vector-Meson Dominance and High-Energy Electron-Proton Inelastic Scattering.*
- [12] N. M. Kroll, T. D. Lee, and B. Zumino, Phys. Rev. **157**, 1376 (1967), *Neutral Vector Mesons and the Hadronic Electromagnetic Current.*
- [13] H. B. O'Connell, B. C. Pearce, A. W. Thomas, and A. G. Williams, Prog. Part. Nucl. Phys. **39**, 201 (1997), *$\rho - \omega$ mixing, vector meson dominance and the pion form-factor.*
- [14] H. Berghauer *et al.*, Phys. Lett. **B701**, 562 (2011), *Determination of the eta-transition form factor in the gamma $p \rightarrow p\eta \rightarrow p\gamma$ e^+e^- reaction.*
- [15] P. Aguar-Bartolome *et al.*, Phys. Rev. **C89**, 044608 (2014), *New determination of the η transition form factor in the Dalitz decay $\eta \rightarrow e^+e^-\gamma$ with the Crystal Ball/TAPS detectors at the Mainz Microtron.*
- [16] R. Arnaldi *et al.*, Phys. Lett. **B757**, 437 (2016), *Precision study of the $\eta \rightarrow \mu^+\mu^-\gamma$ and $\omega \rightarrow \mu^+\mu^-\pi^0$ electromagnetic transition form-factors and of the $\rho \rightarrow \mu^+\mu^-$ line shape in NA60.*
- [17] P. Adlarson *et al.*, Phys. Rev. **C95**, 035208 (2017), *Measurement of the $\omega \rightarrow \pi^0e^+e^-$ and $\eta \rightarrow e^+e^-\gamma$ Dalitz decays with the A2 setup at MAMI.*
- [18] S. Leupold and C. Terschusen, PoS **BORMIO2012**, 024 (2012), *Towards an effective field theory for vector mesons.*
- [19] G. Eichmann, H. Sanchis-Alepuz, R. Williams, R. Alkofer, and C. S. Fischer, Prog. Part. Nucl. Phys. **91**, 1 (2016), *Baryons as relativistic three-quark bound states.*
- [20] J. Staudenmaier, J. Weil, V. Steinberg, S. Endres, and H. Petersen, Phys. Rev. **C98**, 054908 (2018), *Dilepton production and resonance properties within a new hadronic transport approach in the context of the GSI-HADES experimental data.*
- [21] E. Bratkovskaya and W. Cassing, Nucl. Phys. **A807**, 214 (2008), *Low mass dilepton production at ultrarelativistic energies.*
- [22] A. B. Larionov, U. Mosel, and L. von Smekal, Phys. Rev. C **102**, 064913 (2021), *Dilepton production in microscopic transport theory with in-medium ρ -meson spectral function.*
- [23] M. Effenberger, E. L. Bratkovskaya, W. Cassing, and U. Mosel, Phys. Rev. C **60**, 027601 (1999), *e^+e^- pairs from π -A reactions: Comment.*
- [24] M. I. Krivoruchenko, B. V. Martemyanov, A. Faessler, and C. Fuchs, Annals Phys. **296**, 299 (2002), *Electromagnetic transition form factors and dilepton decay rates of nucleon resonances.*
- [25] M. Zetenyi and G. Wolf, Phys. Rev. **C86**, 065209 (2012), *Dilepton production in pion-nucleon collisions in an effective field theory approach.*
- [26] R. Arnaldi *et al.*, Phys. Rev. Lett. **96**, 162302 (2006), *First measurement of the rho spectral function in high-energy nuclear collisions.*
- [27] J. Adamczewski-Musch *et al.*, Nature Phys. **15**, 1040 (2019), *Probing dense baryon-rich matter with virtual photons.*
- [28] L. Adamczyk *et al.*, Phys. Rev. C **92**, 024912 (2015), *Measurements of Dielectron Production in Au+Au Collisions at $\sqrt{s_{NN}} = 200 \text{ GeV}$ from the STAR Experiment.*
- [29] A. Adare *et al.*, Phys. Rev. C **93**, 014904 (2016), *Dielectron production in Au+Au collisions at $\sqrt{s_{NN}}=200 \text{ GeV}$.*
- [30] R. Rapp, G. Chanfray, and J. Wambach, Nucl. Phys. **A617**, 472 (1997), *Rho meson propagation and dilepton enhancement in hot hadronic matter.*
- [31] R. Rapp and J. Wambach, Adv. Nucl. Phys. **25**, 1 (2000), *Chiral symmetry restoration and dileptons in relativistic heavy ion collisions.*
- [32] W. Peters, M. Post, H. Lenske, S. Leupold, and U. Mosel, Nucl. Phys. A **632**, 109 (1998), *The Spectral function of the rho meson in nuclear matter.*
- [33] M. Post, S. Leupold, and U. Mosel, Nucl. Phys. **A741**,

- 81 (2004), *Hadronic spectral functions in nuclear matter*.
- [34] N. P. M. Holt and R. Rapp, *Eur. Phys. J. A* **56**, 292 (2020), *Baryonic Sources of Thermal Photons*.
- [35] P. Salabura and J. Stroth, *Prog. Part. Nucl. Phys.* **120**, 103869 (2021), *Dilepton radiation from strongly interacting systems*.
- [36] J. Adamczewski-Musch *et al.*, *Phys. Rev.* **C102**, 024001 (2020), *Two-Pion production in the second resonance region in π^-p collisions with HADES*.
- [37] J. Adamczewski-Musch *et al.*, *Eur. Phys. J.* **A53**, 188 (2017), *A facility for pion-induced nuclear reaction studies with HADES*.
- [38] G. Agakichiev *et al.*, *Eur. Phys. J.* **A41**, 243 (2009), *The High-Acceptance Dielectron Spectrometer HADES*.
- [39] P. Sellheim, Reconstruction of the low-mass dielectron signal in 1.23A GeV Au+Au collisions, PhD, University of Frankfurt, 2017.
- [40] see Supplemental Material.
- [41] B. Ramstein, *EPJ Web Conf.* **241**, 01012 (2020), *Studying time-like electromagnetic baryonic transitions with HADES in pion induced reactions*.
- [42] A. Sarantsev, *Bonn-Gatchina photoproduction amplitudes*, https://pwa.hiskp.uni-bonn.de/BG2014_02_gn_int.htm.
- [43] F. Scozzi, *Studying excited states of the nucleon with the HADES detector at GSI*, PHD, Paris-Sud and TU Darmstadt universities, 2018.
- [44] B. Friman and H. J. Pirner, *Nucl. Phys.* **A617**, 496 (1997), *P wave polarization of the rho meson and the dilepton spectrum in dense matter*.
- [45] A. Faessler, C. Fuchs, M. I. Krivoruchenko, and B. V. Martemyanov, *J. Phys.* **G29**, 603 (2003), *Dilepton production in proton proton collisions at BEVALAC energies*.
- [46] M. Zétényi, D. Nitt, M. Buballa, and T. Galatyuk, *Phys. Rev. C* **104**, 015201 (2021), *Role of baryon resonances in the $\pi^-p \rightarrow ne+e^-$ reaction within an effective-Lagrangian model*.
- [47] G. Ramalho and M. T. Peña, *Phys. Rev.* **D95**, 014003 (2017), *$\gamma^*N \rightarrow N(1520)$ form factors in the timelike regime*.
- [48] G. Ramalho and M. T. Peña, *Phys. Rev.* **D101**, 114008 (2020), *Covariant model for the Dalitz decay of the $N(1535)$ resonance*.
- [49] K. Nakamura, S. Hiramatsu, T. Kamae, H. Muramatsu, N. Izutsu, and Y. Watase, *Nucl. Phys. A* **268**, 381 (1976), *The Reaction C-12 ($e, e'p$) at 700-MeV and DWIA Analysis*.
- [50] B. W. Allardyce *et al.*, *Nucl. Phys.* **A209**, 1 (1973), *Pion reaction cross-sections and nuclear sizes*.
- [51] M. Lutz, B. Friman, and M. Soyeur, *Nuclear Physics A* **713**, 97 (2003.), *Quantum interference of rho0 and omega-mesons in the $\pi N \rightarrow e^+e^-N$ reaction*.
- [52] A. I. Titov and B. Kämpfer, *Eur. Phys. J.* **A12**, 217 (2001), *Isoscalar-Isovector Interferences in $\pi N \rightarrow Ne^+e^-$ Reactions as a Probe of Baryon Resonance Dynamics*.
- [53] E. Speranza, M. Zetenyi, and B. Friman, *Phys. Lett.* **B764**, 282 (2017), *Polarization and dilepton anisotropy in pion-nucleon collisions*.
- [54] V. V. Sarantsev, private communication.
- [55] G. Ramalho *et al.*, *Phys. Rev.* **D93**, 033004 (2016), *Role of the pion electromagnetic form factor in the $\Delta(1232) \rightarrow \gamma^*N$ timelike transition*.